

Numerical investigation of a two-fluid model for shear-banding polymer solutions

Soroush Hooshyar and Natalie Germann

Fluid Dynamics of Complex Biosystems, School of Life Sciences Weihenstephan,
Technical University of Munich, Germany

ABSTRACT

Shear banding, the formation of localized bands of differing shear rates, is a phenomenon observed in many soft materials. Here we have developed a novel thermodynamically consistent two-fluid model to study steady-state shear banding in semi-dilute entangled polymer solutions. In this model, the formulation of the boundary conditions is straightforward, as the differential velocity is considered as a state variable. The behavior of the model was analyzed for a cylindrical Couette flow and a rectilinear channel flow. We found that stress-induced migration is the diffusive term responsible for the formation of shear bands. The steady-state solution is smooth and unique with respect to different deformation histories and different values of the diffusivity constant. The simplicity of this model makes it attractive for use in more complex flows.

1 INTRODUCTION

Shear banding occurs in soft materials such as wormlike micelles, semi-dilute entangled polymer solutions, and soft glassy materials. Under strong shearing deformations, these fluids can develop inhomogeneous regions in the flow, including multiple localized bands with different shear rates, known as shear bands. Typically, the shear stress of semi-dilute entangled polymers monotonically increases with the shear rate. Several one-fluid reptation models such as the Rolie-Poly model¹ can realistically capture the flow curve and predict transient banding. However, there is experimental evidence for the possibility that shear bands can also exist at steady state.^{2,3} Furthermore, experimental data suggest that polymer solutions can form spa-

tially inhomogeneous concentration profiles.^{4,5} Accordingly, it has been hypothesized that the mechanism giving rise to shear banding is the coupling between the polymer stress and concentration through diffusion.^{6,7}

The two-fluid method is appropriate for investigating diffusional processes in complex fluids. In this approach, it is assumed that the local gradients in concentration and viscoelastic stress generate a difference between the velocities of the polymer and the solvent molecules, which allows them to diffuse at different speeds. Cromer et al⁶ developed a two-fluid model for semi-dilute entangled polymer solutions using kinetic theory. In their model, the diffusive terms were included in the time evolution equation for the polymer concentration. Therefore, to conserve the polymer concentration, a no-flux condition at boundaries was necessary. To construct the other boundary conditions, the differential velocity vanishes at the boundaries. To predict the polymer stress more reliably at rapid deformations, the Rolie-Poly model was used to describe conformational dynamics. Germann et al^{8,9} recently developed a two-fluid approach using the generalized bracket approach of non-equilibrium thermodynamics. The advantage of this new approach is that the differential velocity is treated as a state variable. Consequently, the additional boundary conditions arising from the derivative diffusive terms can be imposed directly with respect to this variable. Furthermore, the description can be easily extended to multiphase systems as the total mass is conserved by the time evolution equations themselves.

Cromer and coworkers studied shear banding in semi-dilute entangled polymer solutions

for Couette flows between parallel plates and concentric cylinders.^{6,7} Although the shear banding behavior of these polymeric systems has yet to be theoretically studied for Poiseuille flows, numerical predictions by the Vasquez-Cook-McKinley (VCM) model are available for wormlike micellar solutions.¹⁰ It was numerically shown for wormlike micelles that above a critical pressure gradient, the velocity profile exhibits a plug-like profile with a high shear band near the walls and a low shear band near the center of the channel. The kink separating these bands is related to the local maximum in the profile of the first normal stress difference. Furthermore, the volumetric flow rate undergoes a spurt as the pressure gradient is increased above a critical value.

Here we aimed to adopt the new two-fluid approach to describe the diffusion banding in semi-dilute entangled polymer solutions within either a cylindrical Couette flow or a Poiseuille channel flow. The remainder of this article is organized as follows. In Sec. 2, we describe the two-fluid method. The behavior of the model is analyzed for the flows in Sec. 3 and the conclusion is drawn in Sec. 4.

2 POLYMER MODEL

In this section, we present a new two-fluid model for semi-dilute entangled polymer solutions developed using the two-fluid framework of generalized bracket approach of nonequilibrium thermodynamics.^{8,9} The total system is considered to be closed, isothermal, and incompressible. This system consists of one polymeric species and one viscous solvent. For the polymer, we define the following variables: the mass density ρ_p , the momentum density $\mathbf{m}^p = \rho_p \mathbf{v}^p$, and the conformation tensor \mathbf{c}^p , defined as the second-moment of the end-to-end vector of the polymer chains. Furthermore, \mathbf{v}^p denotes the velocity field and $n_p = (\rho_p/M_p)N_A$ the polymer number density, with M_p being the molecular weight of the polymer and N_A the Avogadro constant. For the viscous solvent, the following variables are defined: the mass density ρ_s and the momentum density $\mathbf{m}^s = \rho_s \mathbf{v}^s$, where \mathbf{v}^s is the velocity field. The governing

time evolution equations are given as

$$\rho \frac{\partial \mathbf{v}}{\partial t} = -\rho \mathbf{v} \cdot \nabla \mathbf{v} - \nabla p + \nabla \cdot \boldsymbol{\sigma}, \quad (1)$$

$$\frac{\rho_p \rho_s}{\rho} \left(\frac{\partial}{\partial t} + \mathbf{v} \cdot \nabla \right) (\Delta \mathbf{v}) = \frac{\rho_s}{\rho} [-\nabla (n_p k_B T) + \nabla \cdot \boldsymbol{\sigma}^p] - \frac{\rho_p}{\rho} [-\nabla (n_s k_B T) + \eta_s \nabla^2 \mathbf{v}^s] - \frac{G_0}{D} \Delta \mathbf{v}, \quad (2)$$

$$\frac{\partial n_p}{\partial t} = -\nabla \cdot (\mathbf{v}^p n_p), \quad (3)$$

$$\begin{aligned} \frac{\partial \mathbf{c}}{\partial t} = & -\mathbf{v}^p \cdot \nabla \mathbf{c} + \mathbf{c} \cdot \nabla \mathbf{v}^p + (\nabla \mathbf{v}^p)^T \cdot \mathbf{c} \\ & - \frac{1}{\lambda_1} \left[(1-\alpha) \mathbf{I} + \alpha \frac{K}{k_B T} \mathbf{c} \right] \cdot \left(\mathbf{c} - \frac{K}{k_B T} \mathbf{I} \right) \\ & + \frac{1}{\lambda_2} \left[\text{tr} \left(\frac{K}{k_B T} \mathbf{c} \right) - 3 \right]^q \left(\mathbf{c} - \frac{K}{k_B T} \mathbf{I} \right) \\ & + D_{nonloc} \left(\mathbf{c} \cdot \nabla (\nabla \cdot \boldsymbol{\sigma}^p) + [\nabla (\nabla \cdot \boldsymbol{\sigma}^p)]^T \cdot \mathbf{c} \right). \end{aligned} \quad (4)$$

Eq. (1) is the Cauchy momentum balance, with t being the time, $\rho = \rho_p + \rho_s$ the total constant mass of the polymer solution, p the pressure, \mathbf{v} the total average velocity of the polymer solution, and $\boldsymbol{\sigma}$ the total extra stress. Eq. (2) is the time evolution equation for the differential velocity $\Delta \mathbf{v}$, where K is the modulus of elasticity, k_B the Boltzmann constant, T the absolute temperature, η_s the viscosity of the solvent, G_0 the modulus of elasticity, D the diffusivity constant, and $\boldsymbol{\sigma}^p$ the extra stress associated with the polymer. The divergence of $\boldsymbol{\sigma}^p$ accounts for the stress-induced migration and the spatial gradients of the number densities describe the Fickian diffusion. Eq. (3) is the time evolution equation for the polymer concentration. It is a material derivative that accounts for the fact that the polymer concentration can vary locally. Eq. (4) is the time evolution equation for the conformation of the polymer. The left-hand side and the first three terms on the right-hand side constitute the upper-convected time derivative. The fourth term on the right-hand side is the Giesekus relaxation accounting for hydrodynamic interactions, with α being the anisotropy factor. This term was added to capture the overshoot of the shear stress during the start-up of a simple shearing flow triggering the shear band formation. The fifth term in Eq. (4) is a nonlinear relaxation term that we added to capture the upturn of the flow curve at high shear rates. The power-law pre-factor

$[K/(k_B T)\text{tr}\mathbf{c} - 3]^q$ is a scalar function of the trace of the conformation tensor, which is a relative measure for polymer extension. Note that this term closely resembles the term used in the Rolie-Poly model to describe convective constraint release including chain stretch.¹ The last term of Eq. (4) controls the smoothness of the profiles according to the value of the nonlocal diffusivity D_{nonloc} . The time evolution equations are closed by an explicit expression for the extra stress

$$\begin{aligned}\boldsymbol{\sigma} &= \boldsymbol{\sigma}^p + \eta_s \left[\nabla \mathbf{v}^s + (\nabla \mathbf{v}^s)^T \right] \\ &= n_p (K \mathbf{c} - k_B T \mathbf{I}) + \eta_s \left[\nabla \mathbf{v}^s + (\nabla \mathbf{v}^s)^T \right],\end{aligned}\quad (5)$$

where the first term accounts for the viscoelastic stress associated with the polymer and the second term for the contribution of the viscous solvent. The phase velocities associated with the polymer and the solvent can be calculated using the total average velocity and the differential velocity as follows:

$$\mathbf{v}^p = \mathbf{v} + \frac{\rho_s}{\rho} \Delta \mathbf{v},\quad (6)$$

$$\mathbf{v}^s = \mathbf{v} - \frac{\rho_p}{\rho} \Delta \mathbf{v}.\quad (7)$$

In the new model, the differential velocity is considered as a state variable. The extra boundary conditions arising from the derivative terms appearing in Eq. (2) can be directly formulated with respect to this variable. For instance, no-slip and no-penetration conditions are recovered if the tangential and normal components of the differential velocity are set to zero at the walls, respectively. Furthermore, the additional stress-diffusive term appearing in Eq. (4) requires special treatment on the boundaries. We set the parameter D_{nonloc} equal to zero on the solid walls since diffusion should vanish at these locations within a distance less than the radius of the Gyration because of local surface effects.

We worked with dimensionless quantities. Location is scaled by the characteristic length H , time is scaled by the characteristic relaxation time $\tilde{t} = t/\lambda_1$, the extra stress and the conformation tensor are scaled as $\tilde{\boldsymbol{\sigma}} = \boldsymbol{\sigma}/G_0$

and $\tilde{\mathbf{c}} = (K/k_B T)\mathbf{c}$, respectively, where $G_0 = n_p^0 k_B T$. The dimensionless parameters with respect to these scalings are the elasticity number $E = G_0 \lambda_1^2 / \rho H^2$, the ratio of the molecular weight of the solvent to that of the polymer $\chi = M_s / M_p$, the polymer initial concentration $\mu = n_{peq} / (n_{peq} + \chi n_{seq})$, where n_{peq} and n_{seq} denote the polymer and the solvent number densities at the equilibrium state of rest, respectively, the viscosity ratio $\beta = \eta_s / \eta_0$, the ratio of the characteristic relaxation times $\varepsilon = \lambda_1 / \lambda_2$, and the local and nonlocal diffusivity constants $\tilde{D} = D \lambda_1 / H^2$ and $\tilde{D}_{nonloc} = D_{nonloc} \lambda_1 / H^2$, respectively.

3 RESULTS AND DISCUSSION

The model was solved for a cylindrical Couette flow and a Poiseuille channel flow. The model parameters were determined by fitting to the steady shear rheology of a 10 wt/wt% (1.6M) polybutadiene solution.¹¹ The flow problem was solved using a Chebyshev pseudospectral procedure with 200 discretization points as described in Refs.^{8,9,12}

For the cylindrical Couette flow, we used the cylindrical coordinate system as the reference frame. The characteristic length is given as $H = R_o - R_i$, where R_o and R_i are the radii of the outer and inner cylinders, respectively. Subsequently, we take the normalized coordinate $\tilde{r}^* = (r - R_i) / H$ to indicate the location in the cylindrical gap. The outer cylinder is kept stationary, whereas the inner cylinder rotates with the azimuthal velocity specified as in Refs.:^{8,9}

$$\tilde{v}_\theta(\tilde{r}^* = 0, \tilde{t}) = Wi \tanh(\tilde{a} \tilde{t}).\quad (8)$$

Here, \tilde{a} denotes the dimensionless ramp rate of the rheometer and $Wi = \lambda_1 V / H$ the Weissenberg number with V being the dimensional angular velocity.

Fig. 1 shows the steady-state profile of the polymer number density with and without the stress-induced migration. It is obvious that stress-induced migration is responsible for the occurrence of the shear bands. The horizontal line indicates that the polymer number density is nearly uniform across the cylindrical gap if the stress-induced term is ignored.

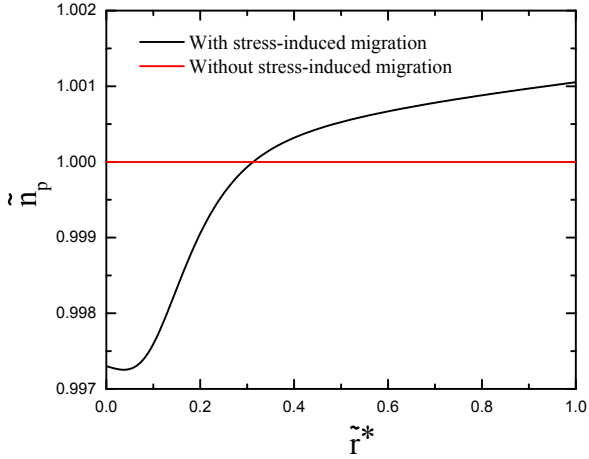


Figure 1. The number density of the polymer is calculated for the model with and without the term corresponding to stress-induced migration. The values of the model parameters used in the calculation were $\alpha = 0.73$, $\varepsilon = 0.0025$, $q = 1.46$, $Wi = 6$, $\beta = E^{-1} = 10^{-5}$, $\mu = \chi = 10^{-1}$, and $\tilde{D} = \tilde{D}_{nonloc} = 10^{-3}$.

Figure 2(a) and 2(b) display the effect of the Weissenberg number on the steady-state profiles of the velocity and polymer number density, respectively. Two distinct shear bands can be seen for $3 < Wi < 63$. If we increase the Wi parameter, the kink separating the bands moves from the rotating inner wall to the stationary outer wall. The profile of the polymer concentration is banded, which is in contrast to the predictions of standard polymer models. The curvature of the geometry justifies the curved shape of this profile.

Figure 3 shows how the deformation history affects the steady-state profile of the polymer number density. This was determined by ramp-up and ramp-down tests. We started the ramp-up test from rest and the ramp-down test from the steady-state solution at $Wi = 100$. A unique steady-state solution was obtained independent of the deformation history.

Figure 4 shows the effect of the nonlocal diffusivity constant \tilde{D}_{nonloc} on the steady-state velocity profile. The profile is smoother for larger values of \tilde{D}_{nonloc} .

For the Poiseuille flow in a rectilinear chan-

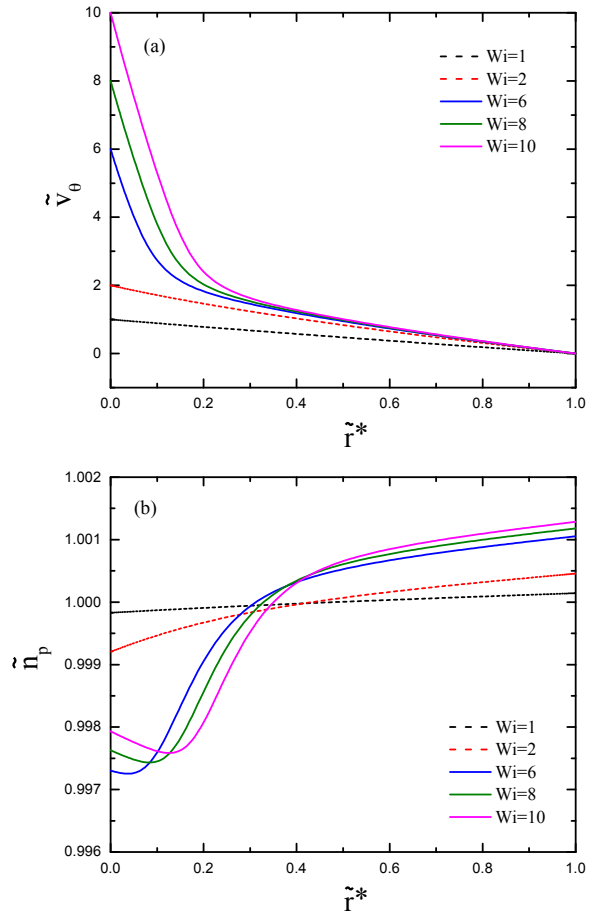


Figure 2. The profiles of (a) the velocity and (b) the polymer number density calculated for different Weissenberg numbers. The other model parameters are the same as those given in the legend of Figure 1.

nel, we used the cartesian coordinate system with the origin at the centerline. The walls are kept stationary whereas a nonzero dimensionless pressure gradient $\tilde{P}_x = \Delta p H / LG_0$ is applied in the x -direction. To avoid unnecessary computations, we solved the model for half of the channel.

Figure 5 shows the effect of the value of the pressure gradient on the steady-state profiles of the velocity and the polymer concentration across the gap. Here, \tilde{y} denotes the location in the channel width, with $\tilde{y} = 0$ and 0.5 corresponding to the centerline and the wall, respectively. The velocity profile forms a low shear rate band near the center and a high shear rate

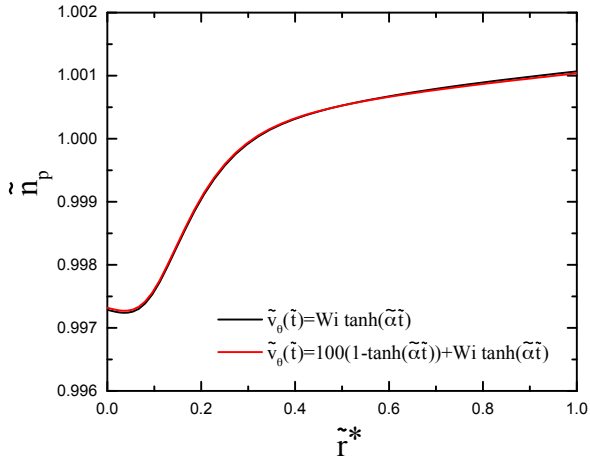


Figure 3. Steady-state profiles of the polymer number density calculated using different deformation histories. The model parameters are the same as those given in the legend of Figure 1.

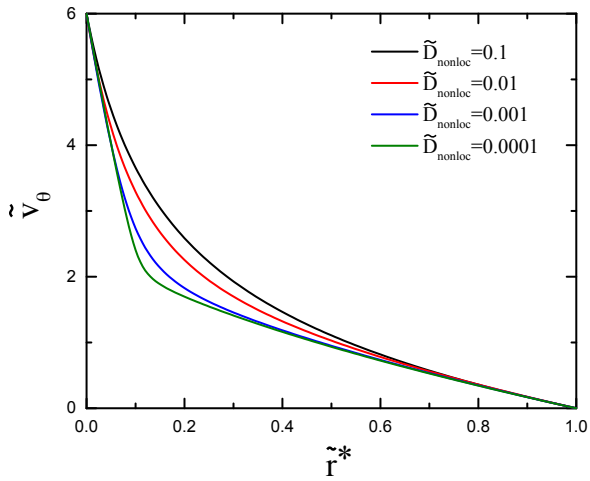


Figure 4. Effect of the nonlocal diffusivity constant on the steady-state profile of the velocity. The other model parameters are the same as those given in the legend of Figure 1.

band near the wall. A striking difference to the predictions of the VCM model is that the transition between the shear bands is smooth even in the case of zero stress diffusion. Furthermore, the plug-like profile is observed over a wider range of the dimensionless pressure gradients (i.e., for $1 < P_x < 200$). The concentration bands are also predicted for the same range. For larger pressure gradients, the polymer con-

centration is more homogeneous with the kink closer to the centerline. It is worth noting that in contrast to the VCM model, this solution is unique for all pressure gradients and no hysteresis is observed in ramp up/down tests.

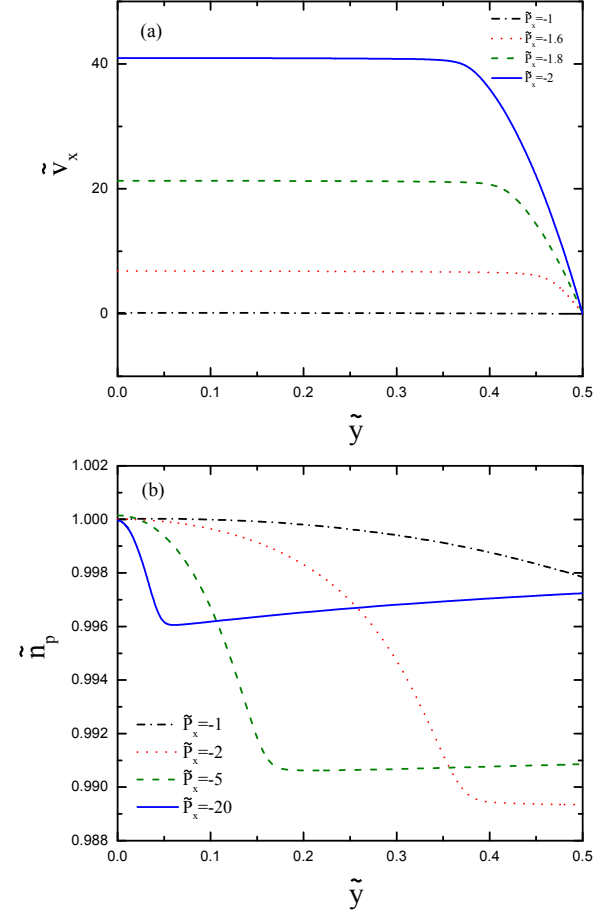


Figure 5. Influence of the pressure gradient on the steady-state profiles of the (a) velocity and (b) polymer concentration across the channel. The values of the model parameters used in the calculation were $\alpha = 0.73$, $\varepsilon = 0.0025$, $q = 1.46$, $\beta = E^{-1} = 10^{-5}$, $\mu = \chi = 10^{-1}$, and $\tilde{D} = \tilde{D}_{nonloc} = 10^{-3}$.

4 SUMMARY AND CONCLUSIONS

Using the generalized bracket approach of nonequilibrium thermodynamics, we have developed a two-fluid model to study shear banding in semi-dilute entangled polymer solutions. Unlike in previous two-fluid models, the differential velocity is treated as a state vari-

able, which makes the specification of the extra boundary conditions straightforward. We used the Giesekus relaxation in the polymer conformation equation to account for hydrodynamic interactions and to capture the overshoot of the shear stress. We added a nonlinear relaxation term to predict the upturn of the flow curve at high shear rates. This term is similar to the term used in the Rolie-Poly model, which describes convective constraint release and chain stretch. Moreover, a stress-diffusive term was added to the conformation equation to control the smoothness of the profiles. We found that the stress-induced migration is the diffusive term responsible for the formation of the shear bands. The steady-state profiles are smooth and unique with respect to applied deformation history and the value of the diffusivity constant. Further boundary conditions such as slip conditions can be easily investigated if the differential velocity is treated as a state variable. The simplicity of our model makes it attractive for the study of complex flows.

ACKNOWLEDGMENT

The authors gratefully acknowledge the financial support of the Max Buchner Research Foundation.

REFERENCES

1. A. E. Likhtman and R. S. Graham. Simple constitutive equation for linear polymer melts derived from molecular theory: Rolie-poly equation. *J. Non-Newton. Fluid Mech.*, 114(1):1–12, 2003.
2. M. Harvey and T. A. Waigh. Optical coherence tomography velocimetry in controlled shear flow. *Physical Review E*, 83(3):031502, 2011.
3. S. Ravindranath, S. Q. Wang, M. Olechnowicz, and R. P. Quirk. Banding in simple steady shear of entangled polymer solutions. *Macromolecules*, 41(7):2663–2670, 2008.
4. M. J. MacDonald and S. J. Muller. Experimental study of shear-induced migration of polymers in dilute solutions. *J. Rheol.*, 40(2):259–283, 1996.
5. A. B. Metzner, Y. Cohen, and C. Rangel-Nafaile. Inhomogeneous flows of non-Newtonian fluids: generation of spatial concentration gradients. *J. Non-Newton. Fluid Mech.*, 5:449–462, 1979.
6. M. Cromer, M. C. Villet, G. H. Fredrickson, and L. Gary Leal. Shear banding in polymer solutions. *Phys. Fluids*, 25(5):051703, 2013.
7. M. Cromer, G. H. Fredrickson, and L. Gary Leal. A study of shear banding in polymer solutions. *Phys. Fluids*, 26(6):063101, 2014.
8. N. Germann, L. P. Cook, and A. N. Beris. Investigation of the inhomogeneous shear flow of a wormlike micellar solution using a thermodynamically consistent model. *J. Non-Newton. Fluid Mech.*, 207:21–31, 2014.
9. N. Germann, L. P. Cook, and A. N. Beris. A differential velocities-based study of diffusion effects in shear-banding micellar solutions. *J. Non-Newton. Fluid Mech.*, 232:43–54, 2016.
10. M. Cromer, L. P. Cook, and G. H. McKinley. Pressure-driven flow of wormlike micellar solutions in rectilinear microchannels. *J. Non-Newton. Fluid Mech.*, 166(3):180–193, 2011.
11. S. Cheng and S. Wang. Is shear banding a metastable property of well-entangled polymer solutions? *J. Rheol.*, 56(6):1413–1428, 2012.
12. N. Germann, M. Dressler, and E. J. Windhab. Numerical solution of an extended White-Metzner model for eccentric Taylor-Couette flow. *J. Comp. Phys.*, 230(21):7853–7866, 2011.